The effect of resist dissolution process on pattern formation variability: an *in situ* analysis using high speed atomic force microscopy

Julius Joseph Santillan, Motoharu Shichiri and Toshiro Itani
EUVL Infrastructure Development Center, Inc. (EIDEC)
16-1 Onogawa, Tsukuba, Ibaraki 305-8569, Japan
Phone: +81-29-869-9727 e-mail: julius.santillan@eidec.co.jp

ABSTRACT

This work focuses on the application of a high speed atomic force microscope for the in situ visualization / quantification of the pattern formation phenomenon during resist dissolution. Specifically, this paper discusses on the quantification of various factors (e.g. pattern roughness, defects, etc.) that affect pattern quality. Comparing two typical positive-tone, extreme-ultraviolet lithography resists of dissimilar lithographic performance, results show that the differences in LER between such resists already exists even during the resist dissolution. This implies the significance of the dissolution process in further improving the final LER of lines-and-spaces (L/S) patterns. Moreover, results have shown the effectiveness of applying the same analysis technique in understanding pattern defect dynamics during dissolution, not only for L/S but also for contact hole (CH) patterns. Preliminary investigations on CH pattern formation during dissolution showed position-dependent variabilities / randomness in the timing of CH formation. Such variabilities in timing imply possible pointers in defining the origin of missing CH defects, from the resist dissolution point-of-view.

Keywords: Resist dissolution, in situ analysis, LER during dissolution, contact holes, defect mechanics, high-speed atomic force microscopy

1. INTRODUCTION

Resist materials and processes play a significant role in achieving high-resolution patterns especially for leading edge lithographic technologies such as extreme ultraviolet lithography (EUVL). In controlling the quality (pattern roughness, defects, etc.) of these high-resolution patterns, resist processes are considered as the key.

Resist dissolution is one part of the resist process that has been constantly investigated as this is the first instance where the physical manifestation of such patterns occurs. In this regard, this process step is important in ensuring the formation of high quality patterns. Numerous fundamental studies on resist dissolution have been made in the past and present, to better understand and control the mechanics surrounding this process. [1-7]

The authors have previously reported a unique and direct approach for the analysis of pattern formation during the resist dissolution process. This analysis technique utilizes a high speed atomic force microscope or HS-AFM (Nano Explorer or NEX by Research Institute of Biomolecule Metrology). The HS-AFM was originally developed for the dynamic observation of soft biological samples in liquid,[8] but was considered for application in resist dissolution analysis given its high speed scanning capabilities (maximum speed: 12.5 frames$\cdot$s^{-1}). Since the inception of this *in situ* analysis technique, significant technical advancements in both tool and methodology have been made. Through such improvements, the analysis of half-pitch or 1:1 lines-and-spaces (L/S) patterns, which are considered the de-facto standard in determining resist material lithographic performance, has been made possible.[3]

Recent activities involving this original technique has shifted from the “observation” to the “quantification” of the results obtained. For example, understanding the trends of line edge roughness (LER) formation in comparison to critical dimension (CD) variation during resist dissolution is one point of interest. Another application being considered is in defining line-bridging / pinching defects occurring during resist dissolution.

This paper demonstrates the analysis methods / results for the above mentioned topics. Additionally, this work also presents the first visual observation of contact hole (CH) pattern formation during resist dissolution.

2. EXPERIMENTAL CONDITIONS

2.1 Materials and processes

For these experiments, the EIDEC standard resist (ESR1) [9] was utilized at 50nm film thickness. The ESR1 is a positive-tone EUVL resist composed of a hybrid polyhydroxystyrene(PHS)-methacryl polymer, onium salt type photoacid generator (PAG) and acid quencher. The ESR1 has a relatively large LER compared to high-end EUV resists reported elsewhere.[10-11] Thus, as a point of comparison for the results obtained from this resist, a lithographically enhanced positive-tone hybrid EUVL resist material (referred to as "litho-enhanced resist" from here on) was utilized, also at 50nm film thickness. Ideal doses were applied in obtaining the target 32nm 1:1 L/S patterns used for these experiments. Optimized post application and post exposure bake (PAB and PEB) conditions were used and resist dissolution was carried out using a typical aq. 2.38wt% tetramthylammonium hydroxide (TMAH) developer.

Moreover, for the contact hole analyses presented here, a separate hybrid (PHS-methacryl polymer) model EUVL resist material was utilized at a film thickness of 60nm. Optimized PAB / PEB conditions were also used and resist dissolution were also done using an aq. 2.38wt% TMAH developer.

These resist materials were coated on to 300mmφ silicon wafers and were exposed using an in-house EUV small field exposure tool or SFET (Numerical aperture = 0.3) which is linked to a coater / developer track system (Clean track ACT12 by Tokyo Electron) in a chemically controlled environment. The standard illumination condition used was an annular illumination of 0.7 / 0.3 (σouter / σinner). After patterning exposures (and PEB), the target area for analysis in the silicon wafer is cleaved to obtain the 2 mm × 2 mm HS-AFM samples.

For these experiments, HS-AFM image scanning was performed over an area of 1000 nm × 1000 nm (at 400 × 400 pixels). This was done at an optimized scan rate of 0.5 frames$\cdot s^{-1}$. "Biolever fast" cantilevers (BL-AC10FS-A2 by Olympus) equipped with carbon nano-fiber tips (radius of curvature: ~7nm) were utilized.

For the experimental procedure [12] with the HS-AFM, the first step is to look for the target pattern, in-liquid (in this case; de-ionized water or DIW). After determining the exact position of the resist pattern, the developer solution is injected continuously into the analysis area while the DIW is being dispensed in the same rate (using an auto-inject-dispense module). This allows continuous and stable scanning of the pattern surface even as the DIW is replaced with the developer solution. However, during this process step, a temporary dilution of the standard developer solution occurs. This temporary dilution of the developer allows a slower, clearer observation of the initial stages of the pattern formation process but in effect, also extends the total resist dissolution process time, in comparison to typical values used in actual resist processes.

All HS-AFM measurements and related sample preparations were performed in a controlled environment inside a class 1 clean room.

2.2 Analysis methodology

In typical HS-AFM results, multiple images obtained represent the state of the target resist film area (where pattern is located) at different times during the dissolution process. As with most AFMs, such images contain three-dimensional data (x, y, z coordinates) which allows the extraction of line LER and CD at specific pattern heights. In this paper, these specific pattern heights are referred to as $Z_{threshold}$ or Z_t. [13] The Z_t convention applied in the discussions sets the resist line pattern's top surface at 0nm with consideration for pattern surface thickness-loss during dissolution. Moreover, to minimize the effect of cantilever size / shape on LER and CD measurements, image de-convolution was performed based on the specifications for the cantilever utilized.[14]

These analyses were specifically focused on the left LER, as the right side-wall of the pattern had evidence of noise due to what is referred to as hunting effect [15] (a type of oscillation occurring in systems utilizing proportional-integral-derivative or PID controllers) which occurs as the scanning probe "climbs" the pattern wall. Line width roughness is also not discussed for the same reason. The LER values shown are the average of the 3σ of each of the 5 lines at the center of each image. Even in the presence of such noise, a rough estimate of the line CD is possible. Line CD was also obtained as the average of 5 lines used in LER analysis.

Moreover, based on the same data set obtained for the above mentioned analyses, the number of line bridging / pinching can also be extracted. For the results discussed in this paper (where patterns were exposed at the ideal doses for 32nm 1:1 L/S), such line bridging and pinching mostly occurred at the beginning and final stages of the resist dissolution process, respectively. These factors appear as successive blank gaps in the data set for each line pattern and are counted as groups forming one line-bridge or pinch.

3. RESULTS AND DISCUSSIONS

3.1 HS-AFM experimental results

Figure 1 shows the *in situ* pattern formation analysis results of a 32 nm 1:1 L/S pattern exposed on the ESR1 (2D and 3D images at the upper bracket) and litho-enhanced resist (2D and 3D images at the lower bracket) during dissolution in aq. 2.38wt% TMAH developer, at various dissolution times.

For both resist materials, the existence of film "swelling" for the exposed areas (pattern space) was confirmed at around t=6s to 12s or the early stages of resist dissolution. Pattern spaces start to appear at the t=12s mark, when exposed areas begin to dissolve in the developer solution after swelling. At these early stages of the dissolution process, the presence of bridging connecting line patterns was observed to occur for both resists. At extended dissolution times (t=58s to t=76s), evidence of line pinching was observed, as visually indicated by the existence of relatively darker spots above the line patterns.

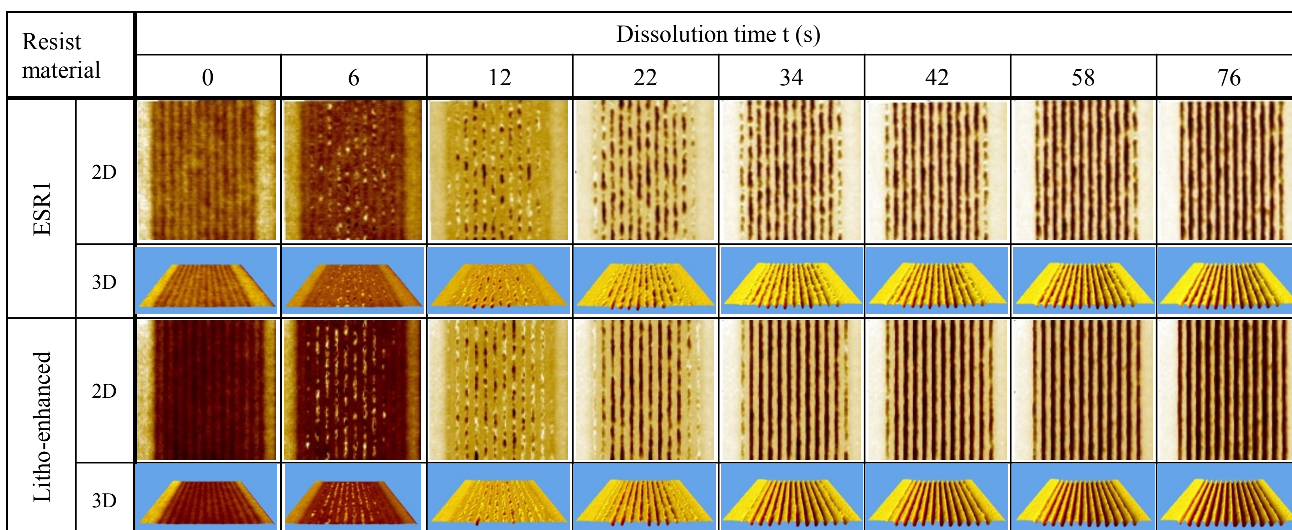

Fig. 1 The *in situ* pattern formation analysis results of a 32 nm 1:1 L/S pattern exposed on the ESR1 (2D and 3D images at the upper bracket) and litho-enhanced resist (2D and 3D images at the lower bracket) during dissolution in aq. 2.38wt% TMAH developer, at various dissolution times.

3.2 LER and CD formation during dissolution

Figure 2 shows the LER and CD analyses results for the 32 nm 1:1 L/S pattern at both (a) ESR1 and (b) litho-enhanced resists during dissolution. White circles and black squares represent the LER and CD trends, respectively. For easier visual appreciation, pattern CD and LER are indicated separately at the left and right Y-coordinates of the graph, respectively. The results shown in this graph have been obtained with Z_t = -10nm, which is the Z_t parameter where obtained pattern CDs are closest to the CD-SEM results measured at 50% threshold. Moreover, it is noteworthy that the values presented in the graphs are taken only for specific dissolution times where the lines are measurable (dissolution times where line bridging are relatively minimal). This explains why measured values only start to appear after more than 10s after dissolution occurs.

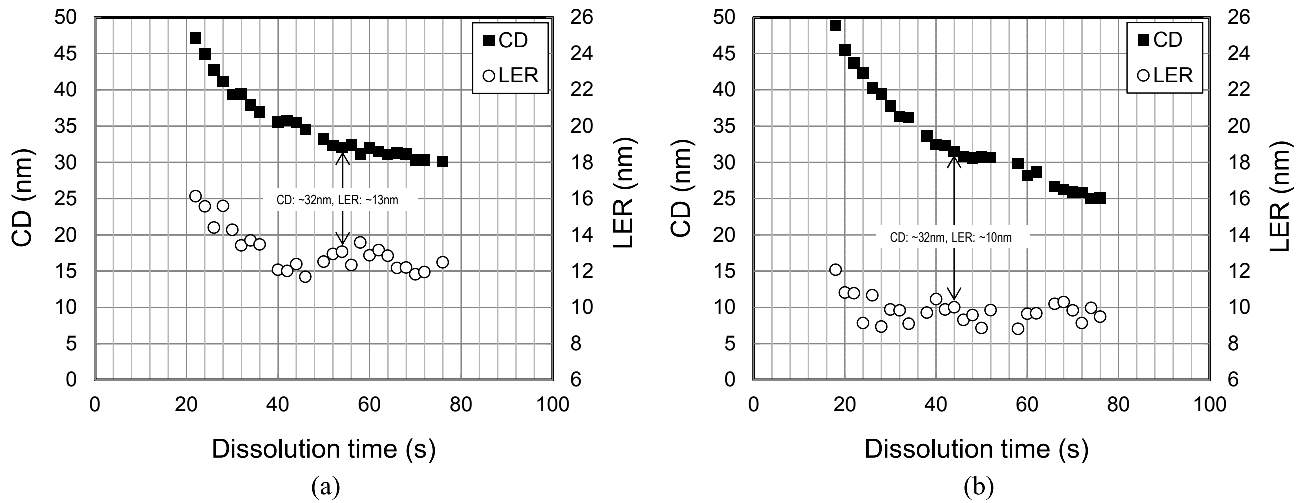

(a) (b)

Fig. 2 LER and CD analyses results for the 32 nm 1:1 L/S pattern at both (a) ESR1 and (b) litho-enhanced resists during dissolution.

As shown in fig. 2(a) for the ESR1 resist, the pattern CD starts off large (CD at ~47nm) during the initial stages of resist dissolution. As dissolution time advances, CD slimming continuously occurs up to the final stages of the dissolution process (CD at ~30nm). For LER, the measured results were observed to decrease from a large value of ~16nm down to ~9.5nm at a certain point in dissolution time (t=40s). At longer dissolution times, LER was observed to fluctuate between ~9.5nm and ~13.5nm. At the dissolution time where target CD size (32nm) is achieved, the LER was ~13nm. These results suggest the presence of an optimal dissolution time in achieving improved LER for a specific resist pattern.

In comparison, using the same measurement method for the litho-enhanced resist as shown in fig. 2(b), a similar CD slimming trend was observed throughout the total dissolution time (starting off with CD at ~49nm and ending with CD at ~25nm). Similar to the ESR1 resist, there was also an LER reduction trend at the early stages of resist dissolution where LER values were at ~12nm (at t=18s) but was reduced to ~9nm after longer dissolution time (at t=28s). More importantly though, the LER values were observed to be relatively lower (LER at optimal CD size of 32nm was ~10nm) compared to those with the ESR1 resist.

Figure 3 summarizes the LER values obtained (left) ”during dissolution” using the HS-AFM at a specific dissolution time where CD size is equal to the target size of 32nm 1:1 L/S compared to those (right) “after drying” using the CD-SEM. These results show that the difference in pattern LER between resists as observed in CD-SEM (after drying) are already existent even during the dissolution process. This implies that to further push pattern LER improvement, manipulation of the dissolution process will be necessary (e.g. dissolution time optimization, alternative dissolution developers or techniques, etc.).

It should be pointed out though that the results using the CD-SEM were completely processed inside the coater / developer tool where resist dissolution is carried out using the puddle development technique. In this regard, the dissolution process is done differently compared to those obtained with the HS-AFM. However, even with such differences in resist processing and measurement methodologies, the undeniably large difference between “during dissolution” and “after drying” LER suggests the significance of the steps between dissolution and drying (e.g. rinse and spin-drying)[16] in reducing the final LER.

Resist material		LER measurement	
		during dissolution (@HS-AFM: Zt = -10)	after drying (@CD-SEM: 50% threshold)
ESR1	Image		
	LER (nm)	~13	5.5
Litho-enhanced	Image		
	LER (nm)	~10	3.5

Fig. 3 LER values obtained (left) "during dissolution" using the HS-AFM at a specific dissolution time where CD size is equal to the target size of 32nm 1:1 L/S compared to those (right) "after drying" using the CD-SEM.

3.3 Line bridging and line pinching defects

As mentioned in chapter 2.2, using the same data set utilized for LER and CD analysis, the analyses of line bridging / pinching was carried out. The ESR1, which showed visual evidence of both line bridging and pinching, was selected for these preliminary analyses. Figure 4, shows the line bridging / pinching analyses results for the 32nm 1:1 L/S patterns exposed on the ESR1 resist. The analyses results at three (3) Z_t conditions are shown; with Z_t = -5nm (white bars at the front edge of the graph) as the condition nearest the pattern top surface, Z_t = -10nm at median (gray bars), and Z_t = -15nm (black bars at the back edge of the graph) as the condition nearest the pattern

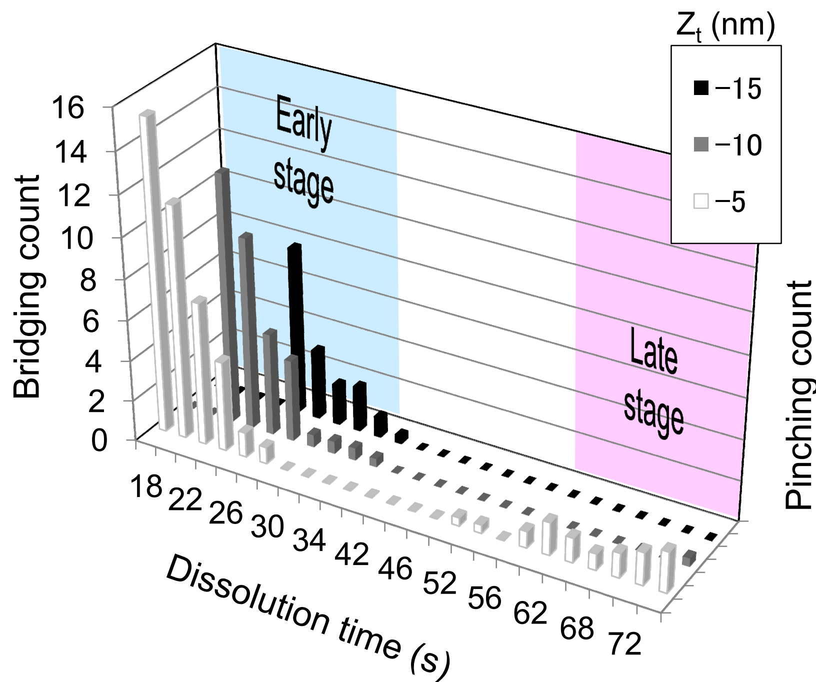

Fig. 4 Line bridging / pinching analyses results for the 32nm 1:1 L/S patterns exposed on the ESR1 resist.

bottom.

From these results, line bridges were detected to first appear at the shallower condition of Z_t = -5nm (t=18s to t=28s). After a few seconds into pattern formation during the dissolution process, line bridges also start to get detected at the Z_t = -10nm condition (t=22s to t=36s). Then lastly, a few seconds later, such line bridges also get detected at Zt = -15nm condition (t=26 to t=36s). This delay in the detection of line bridges depending on the depth of the Z_t condition was expected as line bridges in deeper Z_t values are not detected until line bridges in the shallower Z_t conditions are dissolved. More importantly though is that the existence of such line bridging explains the occurrence of larger LER values in these early stages of dissolution time (as discussed in chapter 3.2). These results also show that LER values decreases as these line bridges dissolve at longer dissolution times.

No line bridging was detected between t=40s to t=50s. However, after a longer dissolution time (t=>52s), similar gaps in the line pattern data were observed. These gaps can be defined as line pinching which is more prevalent at the shallow Z_t condition of -5nm, and not at Z_t = -10 and below. This means that for this resist, such line pinching occurs at the resist surface but not necessarily throughout the line pattern height (even at extended dissolution times). These results suggest that the line pinching observed here is more likely dissolved resist material near the line pattern surface. Such dissolution of the pattern top surface during resist dissolution may translate to larger LER, depending on the Z_t utilized for measurement. It also shows that for this resist, line pinching can occur even at ideal exposure doses for the target pattern size. However, such line pinching can be avoided by limiting / optimizing the dissolution time.

3.4 CH pattern formation during dissolution

Figure 5 shows the *in situ* analysis of CH pattern formation during resist dissolution of a positive-tone hybrid (PHS-methacryl polymer) model resist in aq. 2.38wt% TMAH developer, at various dissolution times; (upper bracket) 32nm 1:1 CH and (lower bracket) 60nm 1:3 CH.

For this resist, a film thickness loss of 2~3nm was observed on the areas where the CH patterns have been exposed (t=0s), even before resist dissolution starts. This specific resist has been known to exhibit swelling (in the exposed areas) before dissolution into the developer solution.[16] Thus, as expected, the exposed CH was observed to swell (t=20s and beyond) for both pattern formats investigated.

However, it is interesting to note how the occurrence of swelling for each CH happens at different timings. This consequently affects the timing of hole formation after the swelled areas are dissolved. At longer dissolution times; t=82s (for 32nm 1:1 CH) and t=48s (for 60nm 1:3 CH), all the CHs observed for both pattern formats were dissolved. However, such randomness in CH formation timing suggests the possibility of position-dependent variabilities in the occurrence of chemical reactions (e.g. presence or absence of deprotected polymers, etc.) necessary for the dissolution / formation of each of these holes. Defining such phenomena may provide pointers in

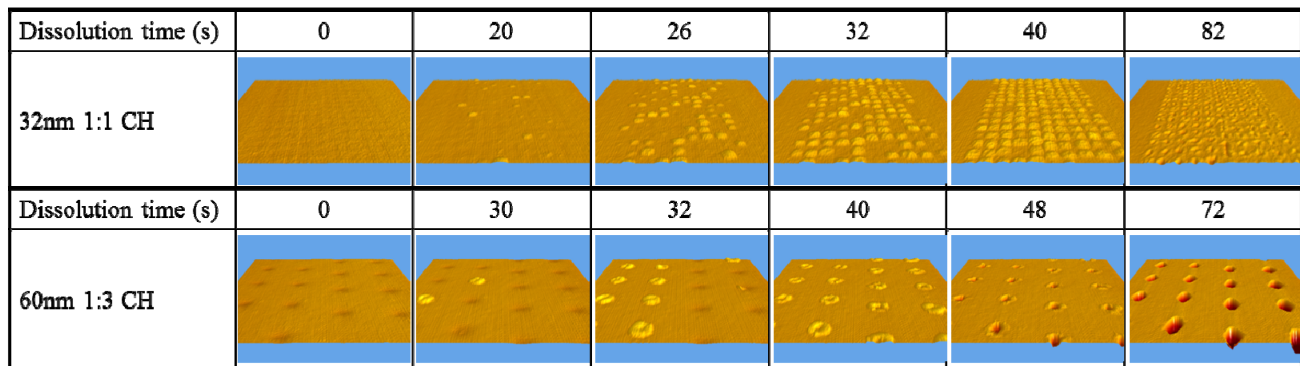

Fig. 5 *In situ* analysis of CH pattern formation during resist dissolution of a positive-tone hybrid (PHS-methcryl polymer) model resist in 2.38wt% TMAH developer, at various dissolution times; (upper bracket) 32nm 1:1 CH and (lower bracket) 60nm 1:3 CH.

understanding the origin of missing CH defects, from the resist dissolution point-of-view.

4. SUMMARY

The observation and quantification of various factors (e.g. LER, line-bridging / pinching) affecting pattern quality during resist dissolution was successfully demonstrated using the HS-AFM based *in situ* analysis technique. Comparing two typical positive-tone EUV resists of dissimilar lithographic performance, results obtained show that the differences in LER between such resists already exists even during the dissolution process. This implies the significance of the dissolution process in further improving the final LER of L/S patterns. Moreover, results have also shown the effectiveness of applying the same analysis technique in understanding pattern defect dynamics during dissolution, not only for L/S but for also CH patterns. Preliminary investigations on CH pattern formation during dissolution showed position-dependent variabilities / randomness in the timing of CH formation. Such variabilities in timing imply possible pointers in defining the origin of missing CH defects, from the resist dissolution point-of-view.

ACKNOWLEDGEMENTS

This work was supported by the New Energy and Industrial Technology Development Organization (NEDO). We would like to thank EIDEC member companies (Advanced resist research program) for their continued support and resist and material manufacturers for providing the latest resist technologies.

REFERENCES:

[1] Sanchez, M., Sundberg, L., Wallraff, G., Hinsbergb, W., Bozanoa, L., Truonga, H., and Petrillo, K., "Monitoring the evolution of line edge roughness during resist development using an analog of quenched flow kinetics," *Proc. SPIE* **8682**, 868218 (2013).

[2] Fonseca, C., Head, B., Shite, H., Nafus, K., Gronheid, R., and Winroth, G., "Understanding EUV resist dissolution characteristics and its impact to RLS limitations," *Proc. SPIE* **7969**, 796911 (2011).

[3] Itani, T. and Santillan, J.J., "In situ Characterization of Photoresist Dissolution," *Appl. Phys. Express* **3**, 061601 (2010).

[4] Hinsberg, W., Houle F., Lee S.-W., Ito H., and Kanazawa K., "Characterization of Reactive Dissolution and Swelling of Polymer Films Using a Quartz Crystal Microbalance and Visible and Infrared Reflectance Spectroscopy," *Macromolecules* **38**, 1882 (2005).

[5] Kokkinis, A., Valamontes E. S., and Raptis I., "Dissolution properties of ultrathin photoresist films with multiwavelength interferometry," *J. Phys.* **CS10**, 401 (2005).

[6] Singh, L., Ludovice, P., and Henderson, C., "Effect of film thickness on the dissolution rate behavior of photoresist polymer thin films," *Proc. SPIE* **5376**, 1007 (2004).

[7] Itani, T., Yoshino, H., Hashimoto, S., Yamana, M., Samoto, N., and Kasama, K., "Polymer structure effect on dissolution characteristics and acid diffusion in chemically amplified DUV Resists," *J. Vac. Sci. Technol.* B **15**, 2541 (1997).

[8] Ando, T., Uchihashi, T., Kodera, N., Yamamoto, D., Miyagi, A., Taniguchi, M., and Yamashita, H., "High-speed AFM and nano-visualization of biomolecular processes," *Pflugers Arch.* **456**, 211 (2008).

[9] Sugie, N., Itani, T., Kozawa, T., "EUV resist simulation based on process parameters of pattern formation reaction," *Proc. SPIE* **9048**, 90482G (2014).

[10] Maruyama, K., Ayothi, R., Hishiro, Y., Inukai, K., Shiratani, M., and Kimura, T., "Novel EUV resist materials and process for 20 nm half pitch and beyond," *Proc. SPIE* **8682**, 86820B (2013).

[11] Tsubaki, H., Tarutani, S., Inoue, N., Takizawa, H., and Goto, T., "EUV resist materials design for 15 nm half pitch and below," *Proc. SPIE* **8679**, 867905 (2013).

[12] Santillan, J.J. and Itani, T., "In situ Analysis of the EUV Resist Pattern Formation during the Resist Dissolution

Process," *J. Photopolym. Sci. Technol.* **26**, 611 (2013).
[13] Santillan, J.J., Shichiri, M., and Itani, T., "In situ characterization of nano-scale pattern roughness during resist dissolution process," *submitted to Microel. Eng.* (2014).
[14] BL-AC10FS-A2 cantiever spec. sheet retrieved from http://probe.olympus-global.com (2014).
[15] Hunting [Def. f] Oxford English Dictionary (2nd ed.). Oxford University Press. 1989. "f. The action of a machine, instrument, system, etc., that is hunting; an undesirable oscillation about an equilibrium speed, position, or state."
[16] Santillan, J.J. and Itani, T., "An in situ analysis of the resist pattern formation process," *Proc. SPIE* **8325**, 83250P (2012).